

Supplementary information

Reusing wastewater for agricultural irrigation: a Nexus approach for Sustainable Development in the North Western Sahara Aquifer System

Camilo Ramirez¹, Youssef Almulla¹, and Francesco Fuso-Nerini¹

¹ KTH Royal Institute of Technology, Stockholm, Sweden

E-mail: camilorg@kth.se

27 November 2020

Contents

1	Geographic Information Systems analysis	1
1.1	Land-cover and cropland area datasets	2
1.2	Population dataset	4
1.3	Depth to groundwater dataset	5
2	Data calibration	5
3	Population and irrigation water withdrawals.	6
4	Groundwater pumping	6
5	Energy-for-wastewater	7
6	Wastewater Treatment System characteristics	7
7	Reverse Osmosis desalination	8
8	Levelised Cost of Water (LCOW)	10
9	Clusters	11
10	Water extractions and reuse per cluster	12
11	Energy demand per cluster	20

1. Geographic Information Systems analysis

Geospatial characteristics of the NWSAS were obtained from open sources as described in table 1. All data layers were converted into matching units, re-projected into the Sud Algerie Degree projection (ESRI: 102592)—This projection was selected as it produces minimal distortions in the analysis area—, re-scaled to the same resolution and, when only individual data points were available, interpolated to extend the data to the entire analysed area (i.e. for the Groundwater quality layer). Furthermore, all layers were merged into a large data frame.

Table 1. Geographic Information System data sources

Layer	Coverage	Format	Resolution	Year	Source
Population	Algeria, Tunisia, Libya	raster (tif)	100 m grid cell	2015	[1]
Depth to groundwater	Africa	txt table	5 km grid cell	2012	[2]
Administrative boundaries	Africa	shapefile	Individual country polygons	2017	[3]
Administrative boundaries	Algeria, Tunisia, Libya	shapefile	Level 1 (provinces) polygons	2015	[4]
Transboundary aquifers borders	Global	shapefile	Individual polygons	2015	[5]
Groundwater quality	NWSAS Basin	data points	206 data points	2016	RA*
Digital Elevation Data*	Africa	raster (tif)	1, 3 and 15 arc second	2014	[6]
Land cover	Africa	raster (tif)	20 m grid cell	2016	[7]
Aquifer boundaries	NWSAS basin	shapefile	Individual polygons	-	RA*
Climate data	Global	raster (tif)	30 arc second, monthly	1970-2000	[8]

* Regional Authorities.

1.1. Land-cover and cropland area datasets

Figure 1 shows the land-cover dataset used for the region. This data was developed by the Land Cover project of the ESA Climate Change Initiative, and consist of a 20×20 m resolution raster for the entire continent of Africa [7]. It classifies land-cover into nine categories: (1) Trees cover area, (2) Shrubs cover area, (3) Grassland, (4) Cropland, (5) Vegetation aquatic or regularly flooded, (6) Lichen Mosses/Sparse vegetation, (7) Bare areas, (8) Built up areas, and (9) Open water.

From this dataset, some insights can already be obtained. Bare/desertic areas dominate the region, while open water bodies are quite uncommon, however, the water bodies found in the NWSAS region do not constitute “fresh water” resources due to their high content of salinity [9]. The built up areas are highly scattered throughout the NWSAS region as well as the cropland zones, which are mainly located in the surroundings of the built up areas and in the north of the region. The largest agricultural activity, is given at the north of the three countries, as well as the major urban concentrations, nonetheless, this does not make the NWSAS region less important, as the groundwater resources there, are crucial for ensuring food security for a growing population in the region.

From this land-cover dataset, the cropland areas were subtracted, allowing to create a raster layer containing the cropland density in the region. This layer was created for a resolution of 1km grid cell and calibrated for year 2015 according to regional statistics presented in Table 2. The obtained cropland dataset is showcased in Figure 2.

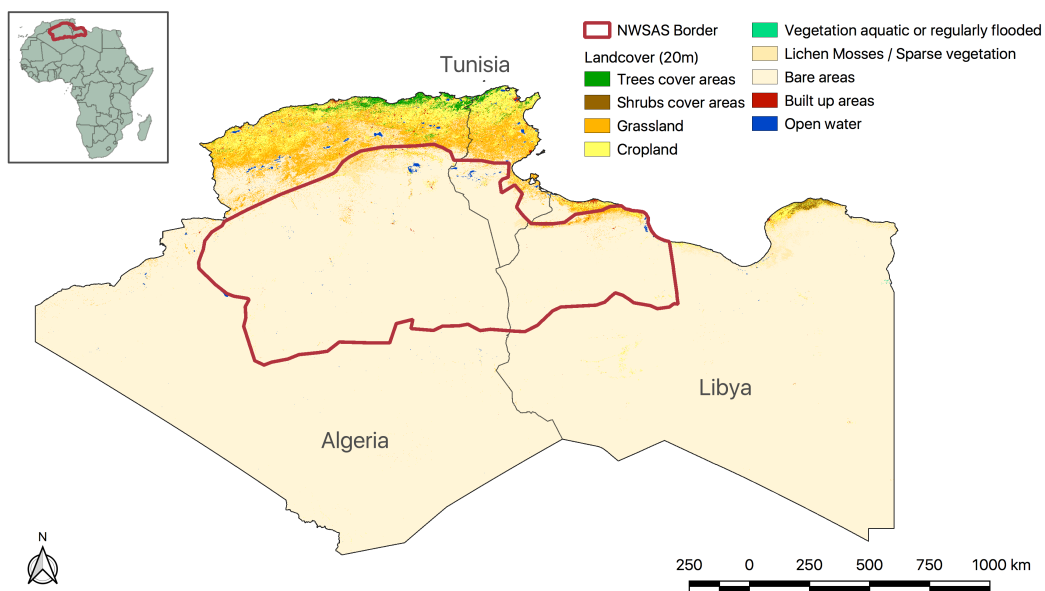


Figure 1. North Western Sahara Aquifer System - Land-cover map at 20×20 meters grid cell resolution.

From Figure 2, it is depicted with more clarity that the main agricultural activity is in fact, presented in the northern region. The provinces with largest agricultural

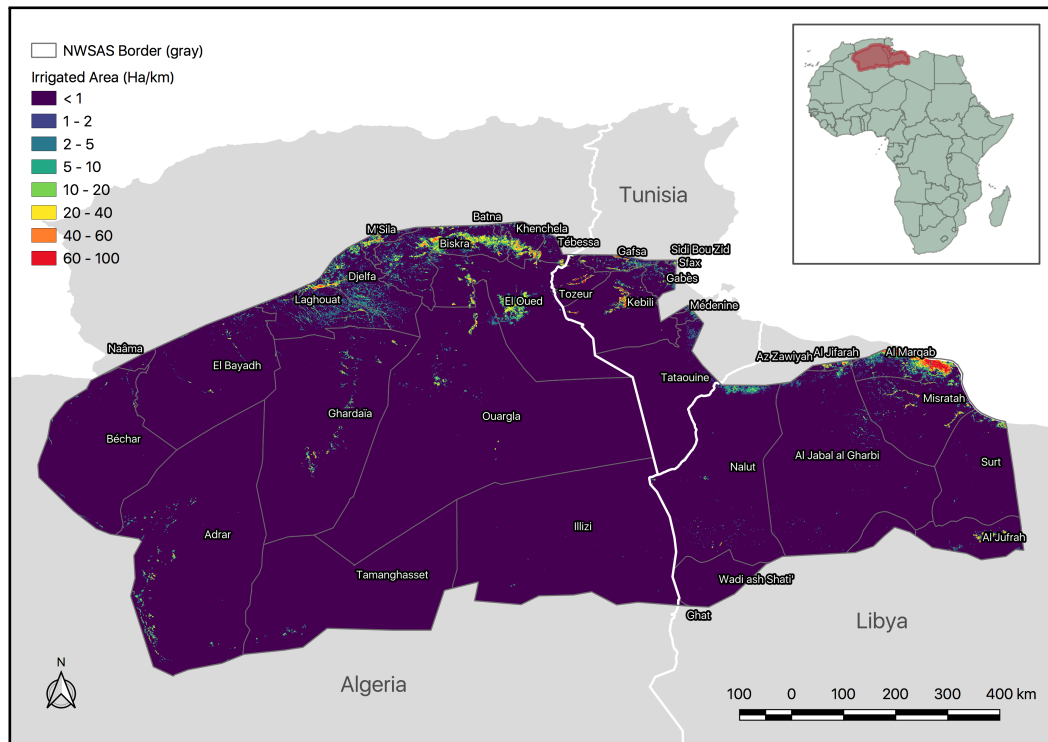


Figure 2. North Western Sahara Aquifer System - Cropland density map at 1×1 km grid cell resolution.

activity are: Biskra, El Oued, Djelfa, Laghouat, Khenchela, Adrar and Ghardaïa in Algeria; Kebili, Tozeur and Gafsa in Tunisia; and Al Marqab, Misratah and Al Jufrah in Libya.

1.2. Population dataset

Individual population datasets for Algeria, Tunisia and Libya were obtained from the WorldPop database [10] in a resolution of 100×100 meters. Afterwards, the three datasets were merged together and masked within the boundaries of the aquifer. The data was then rescaled to a 1 km grid cell resolution and calibrated for year 2015 according to regional statistics (refer to Table 2).

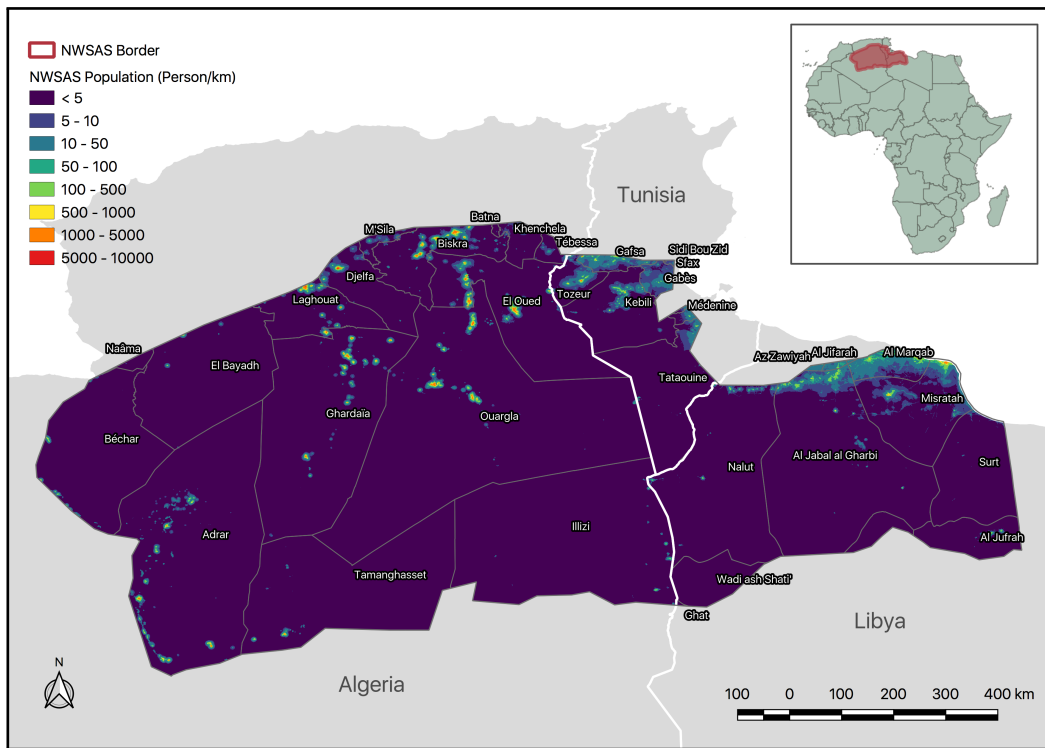


Figure 3. North Western Sahara Aquifer System - Population density map at 1×1 km grid cell resolution.

Figure 3 depicts the obtained population layer for the NWSAS region. It is clear that the population agglomerations follow the same location pattern as the cropland areas: scattered through the region with higher concentrations at north of the aquifer. Within Algeria, the provinces with major population count are: Biskra , El Oued, Ouargla, Laghouat, Ghardaïa, Adrar and Djelfa. As for Tunisia, Kebili, Tozeur and Gafsa present the higher population counts, although much lower than the Algerian provinces previously mentioned. Moreover, the provinces with higher population count within Libya are Al Marqab, Misratah and Al Jabal al Gharbi.

1.3. Depth to groundwater dataset

The depth to groundwater dataset used, was developed by the British Geological Survey for the African continent at a resolution of 5km grid cell. This dataset is underpinned by dedicated case studies and systematic data and literature reviews [2]. The dataset was masked with the NWSAS boundaries and aligned to match the target 1km grid cell resolution (Figure 4).

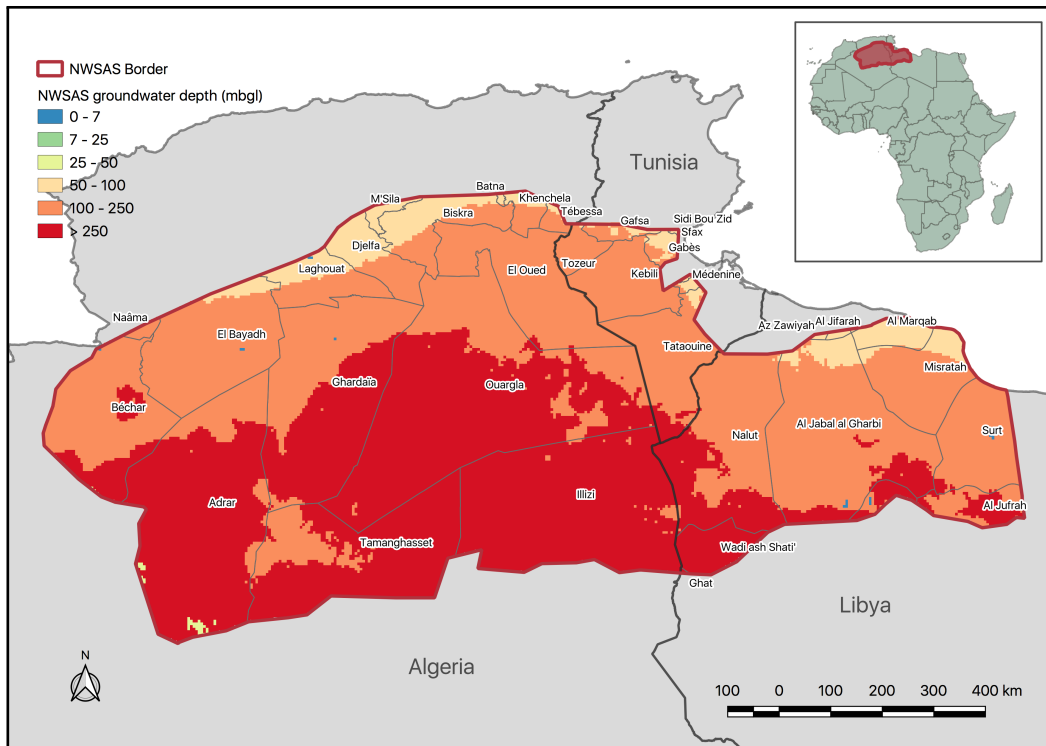


Figure 4. North Western Sahara Aquifer System - Depth to groundwater map at 1×1 km grid cell resolution.

According to this data, it can be seen that the depth to groundwater through the entire aquifer ranges from around 50 to more than 250 meters. In general, in the south of the aquifer the deepest water tables can be found, which could mainly affect the population and agricultural activity of the province of Adrar and part of the provinces of Ouargla and Ghadames. To the north of the basin, the water table levels decrease to a range between 50 to 100 meters, which can be argued, enables the high agricultural activity there, specially in the province of Biskra.

2. Data calibration

The *population* and the *irrigated area* layers were calibrated to match regional statistics. The calibration was performed using the fraction given between the regional statistical data (i.e. total population or total irrigated area), and the sum of all data points of the layer in question. The statistical data was available as per country basis. Thus, the

calibration process was performed for the basin areas within each country, using their specific information (see table 2).

Table 2. NWSAS population and irrigated area statistics for year 2015, subdivided per country area inside the basin. Data source: [11]

Parameter	Total	Algeria	Tunisia	Libya
NWSAS Population	6,376,367	4,240,888	617,168	1,518,311
NWSAS Irrigated area (Ha)	469,529	237,485	56,547	175,497

Moreover, to calibrate the irrigated area data, an algorithm was run to ensure that none of the data cells had more than 100% of its area covered by irrigated land.

3. Population and irrigation water withdrawals

The calculation of total water withdrawals $ww_{tot,i}$ was performed according to (1). Population water withdrawals were calculated as the product between the population count in each data cell (Pop_i) and the specific water demand per capita (wpc_i) for the region. Similarly, withdrawals from irrigated agriculture were calculated as the product between the irrigated area inside each data cell ($IrrArea_i$) and the specific water demand per cultivated hectare ($wpha_i$) for the region.

$$ww_{tot,i} = Pop_i \cdot wpc_i + IrrArea_i \cdot wpha_i \quad (1)$$

For the baseline, a level of water withdrawals per capita wpc of 55 cubic meters per year was assumed with a population growth of 1% per year [12]. Moreover, all cropland area within the aquifer was considered to be irrigated by groundwater resources and the water requirements per cultivated hectare $wpha$ to be 13,520 m³/Ha for the Algerian part; 13,266 m³/Ha for Tunisia and 9,134 m³/Ha for Libya, according to data from [13]. Finally, no growth in irrigated area was considered.

4. Groundwater pumping

The energy needs to pump water from groundwater resources is given by the required lift ($H - h$), the pressure drop due to fluid friction in the piping, and the pressure losses in valves and fittings. Pressure losses due to friction in the piping were found to be rather small compared to the lift requirements. Therefore, and due to lack of specific data on wells and boreholes in the region, the pressure losses due to friction in the piping and in valves and fittings were disregarded. The energy requirements (in watt-h) can then be estimated as (2) [14]:

$$E = \frac{Q \cdot (\rho \cdot g \cdot (H - h))}{\eta} \quad (2)$$

Where Q stands for the water extractions (m^3), ρ for the water density (kg/m^3), g for the gravitational acceleration (m/s^2), H for the delivered hydraulic head (meters), and h for the head in the well (meters). Moreover, η accounts for the pumping efficiency, which was set as 85% along the entire aquifer.

5. Energy-for-wastewater

To calculate the energy-for-wastewater requirements an energy intensity factor was used for each evaluated treatment technology following (3).

$$E_{ww} = Q_{ww, \text{yr}} \cdot X_t \quad (3)$$

Where $Q_{ww, \text{yr}}$ represents the yearly treated wastewater in m^3/yr , and X_t the average energy demand of the specific WWTT t , to treat one m^3 of wastewater (in kWh/m^3).

6. Wastewater Treatment System characteristics

FAO standards for population wastewater pollutant levels and reused water quality for agricultural irrigation [15], were used for the entire NWSAS area. These are shown in table 3.

Table 3. Pollutant levels of wastewater and treated wastewater (mg/l).

Pollutant type	Wastewater	Treated wastewater
Suspended solids (SS)	900	100
Nitrogen (N)	40	10
Phosphorus (P)	20	2
Biochemical Oxygen Demand (BOD_5) (BOD_5)	500	50
Chemical Oxygen Demand (COD)	500	50

Cost functions for different WWTT taken from the work of Molinos-Senante et al. [16], were used to evaluate the competence of selected technologies in the NWSAS. Energy intensity characteristics were added for each technology according to [17, 18]. The characteristics of the different WWTT and their cost and energy functions are presented in table 4.

Table 4. Treatment systems analysed. Adapted from [16] unless otherwise stated.

Technology	Contaminant removal (%)	Costs (€)	Energy (kWh) [‡]	Usage
Pond System (PS)	N: 20 – 40 P: 60 – 70 COD: 60 – 96 SS: 50 – 90	CAPEX: $3897.7 \cdot x^{-0.407}$ OPEX: $5.543 \cdot x + 3127.5$	$0.19 \cdot V$	Irrigation tailwater

continued ...

... continued

Technology	Contaminant removal (%)	Costs (€)	Energy (kWh) [‡]	Usage
Intermittent Sand Filter (ISF)	N: 65 – 95 P: 75 – 99 COD: 75 – 90 SS: 85 – 95	CAPEX: $2115.5 \cdot x^{-0.399}$ OPEX: $12.026 \cdot x + 3518.9$	$0.2 \cdot V$	Population wastewater
Trickling Filter (TF)	N: 35 – 50 P: 35 – 55 COD: 75 – 90 SS: 50 – 90	CAPEX: $12237 \cdot x^{-0.87}$ OPEX: $13.504 \cdot x + 6020$	$0.3 \cdot V$	Population wastewater
Moving Bed Biofilm Reactor (MBBR)	N: 10 – 20 P: 30 – 40 COD: 20 – 40 SS: 60 – 80	CAPEX: $1187 \cdot x^{-0.165}$ OPEX: $12.794 \cdot x + 6031$	$0.8 \cdot V$	Population wastewater
Rotating Biological Contractors (RBC)	N: 20 – 80 P: 10 – 30 COD: 70 – 93 SS: 75 – 98	CAPEX: $6931.4 \cdot x^{-0.383}$ OPEX: $313.4 \cdot x^{-0.435}$	$0.8 \cdot V$	Population wastewater
Membrane Bioreactor (MBR)	N: 50 – 90 P: 20 – 70 COD: 70 – 90 SS: 85 – 99	CAPEX: $5635.3 \cdot x^{-0.352}$ [†] OPEX: $2.116 \cdot V^{0.713} e^{1.51 \cdot SS + 0.037 \cdot BOD}$	$0.8 \cdot V$	Population wastewater
Extended Aeration (EA)	N: 50 – 90 P: 15 – 70 COD: 70 – 90 SS: 85 – 99	CAPEX: $7946 \cdot x^{-0.460}$ [†] OPEX: $169.48 \cdot V^{0.454} e^{0.61 \cdot SS}$	$0.6 \cdot V$	Population wastewater
Sequencing Batch Reactor (SBR)	N: 55 – 90 P: 25 – 70 COD: 70 – 90 SS: 85 – 99	CAPEX: $8258.9 \cdot x^{-0.407}$ OPEX: $309.4 \cdot x^{-0.389}$	$1 \cdot V$	Population wastewater

x : population equivalent, $x = V \times 1500 / (400 \times 365)$, V : wastewater flow (m^3/yr)

N: Nitrogen, P: Phosphorus, COD: Chemical Oxygen Demand, SS: Suspended Solids

CAPEX: Capital Expenditure, OPEX: Operating Expenses

[†] Taken from [19]

[‡] Based on [20, 18]

7. Reverse Osmosis desalination

Reverse Osmosis (RO) desalination is the most popular desalination technology used worldwide. Its energy intensity falls typically in the range of 0.5 to 2.5 kWh per cubic meter of desalinated brackish water [21].

To estimate the energy required to desalinate one cubic meter of saline water, often detailed information of the RO system is required. When analysing a broad area using a geospatial approach, such information is not available as the characteristics of the system can change from application to application [22, 23]. Thus, a simplified approach was used to estimate the RO energy requirements. RO is a pressure-driven

process that forces water through a membrane which separates dissolved solutes using preferential diffusion. The output water from the membrane (*permeate*, *p*) is relatively free of solutes, while the remaining water (*concentrate*, *c*) exits the pressure vessel with a high concentration of solutes (i.e. high TDS levels). A schematic representation of the process is presented in figure 5 [24].

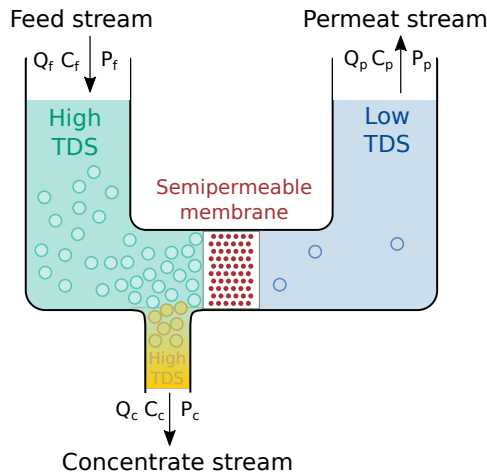


Figure 5. Reverse osmosis schematic separation process. Based on: [24].

The minimum energy required to push the water through the membrane is given by the amount of diluted solutes in the *feed* (*f*) water. Such minimum energy can be estimated calculating the osmotic pressure of the *feed* water, as described in (4) [24].

$$\pi = \phi \cdot C \cdot R \cdot T \quad (4)$$

Where:

- π : osmotic pressure (bar),
- ϕ : osmotic coefficient, close to 1 (-), assumed a 0.95 [24],
- C : concentration of all solutes (mol/L),
- R : universal gas constant, 0.083145 (L·bar/mol·K),
- T : absolute temperature (K), ($273 + {}^{\circ}\text{C}$), assumed at $25 {}^{\circ}\text{C}$ for the entire aquifer.

Thus, the minimum energy demand can be estimated multiplying the osmotic pressure of the *feed* water π (in bar) by a conversion factor of $1.0 \text{ kWh/m}^3 = 36 \text{ bar}$. In reality, the energy demanded is greater due to factors as friction losses, membrane filtration resistance, among others. However, this approach has been used in cases where no specific data of the RO system is available [25].

The water quality layer used, was obtained from 206 measurements provided by National Authorities of the region. Each point specifies the spacial location and groundwater TDS content. Although the data did not cover the entire basin area, due to lack of any other related information it was used to produce a raster layer. An

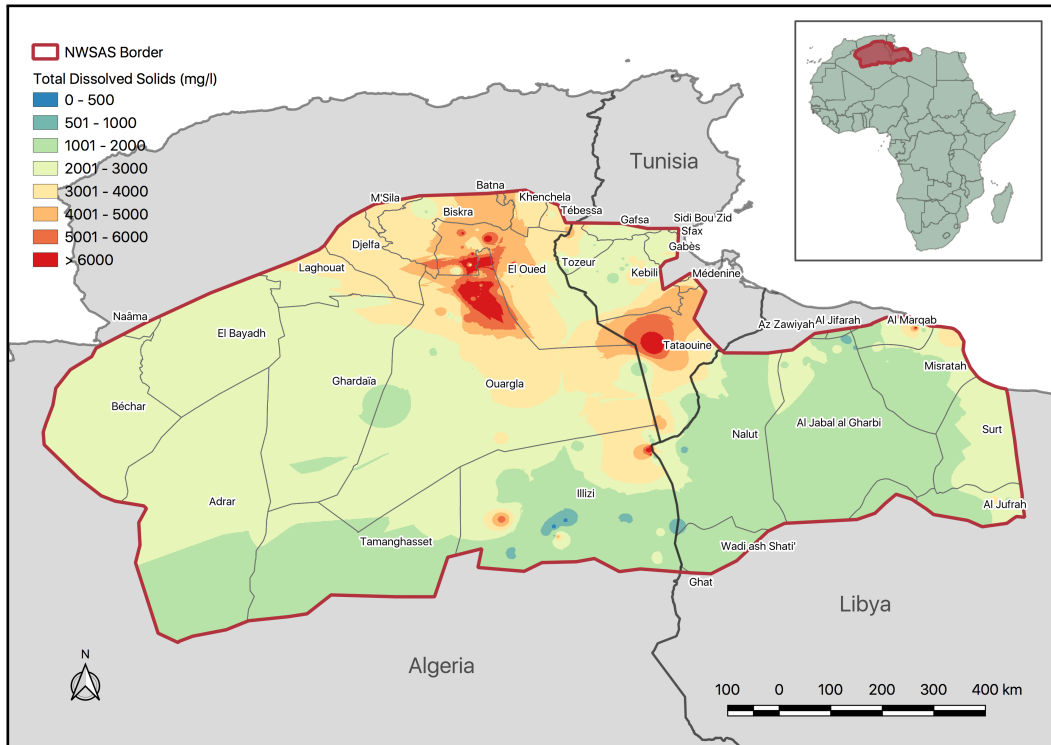


Figure 6. North Western Sahara Aquifer System - Groundwater quality map, Total Dissolved Solids (TDS) at 1×1 km grid cell resolution.

inverse distance weighted interpolation method, having as distance weighting factor an inverse distance to a power of 2 and a global search radius with maximum number of nearest points of 10 was used (see figure 6).

8. Levelised Cost of Water (LCOW)

Equation 5, disaggregates the $LCOW$ ($\$/m^3$) value in three components: the cost components due to investment $LCOW_{Inv}$, operation and maintenance $LCOW_{O\&M}$ and externalities $LCOW_{Ext}$.

$$LCOW = LCOW_{Inv} + LCOW_{O\&M} + LCOW_{Ext} \quad (5)$$

All investment components used, need to be comprised in the CAPEX function of each WWTT. This enables the use of the values calculated with the CAPEX functions of each WWTT for each region or cluster, to easily calculate the $LCOW_{Inv}$ values for each specific technology and region/cluster. Equation 6 describes the process to calculate the $LCOW_{Inv}$.

$$LCOW_{Inv} = \frac{Inv}{\sum_{t=1}^T V_t \cdot \gamma^t} \cdot \Delta \quad (6)$$

Where Inv stands for the CAPEX value, V_t for the treated water flow per year t (m^3/yr), Δ for the tax factor (Equation 8) and γ^t represents the discount factor of the project (Equation 7).

The discount factor is an important term, as the LCOW methodology represents a break-even investment for the stakeholders, thus an appropriate discount rate (r) needs to be used to ensure the right amount of return needed for all sources of long term capital (i.e. equity holders and debt). Often, the proper discount rate used is the WACC [26]. The discount factor is then calculated according to the discount rate r , as shown in (7). A discount rate of $r = 4\%$ was used for this study.

$$\gamma^t = \left(\frac{1}{1+r} \right)^t \quad (7)$$

The tax factor Δ includes all effects of the tax related variables, these being the rent tax α , depreciation d_t , depreciation period T , discount factor γ and investment tax credit i . Equation 8 describes the way of obtaining the tax factor.

$$\Delta = \frac{1 - i - \alpha \cdot \sum_{t=1}^T d_t \cdot \gamma^t}{1 - \alpha} \quad (8)$$

Moreover, the LCOW related to operational costs $LCOW_{O\&m}$ (Equation 9) can be computed by using the OPEX values ω_t calculated for each year, in each region/cluster — using the cost-functions of each WWTT evaluated—the treated water flow V_t (m^3/yr) and the discount factor γ^t per year.

$$LCOW_{O\&m} = \frac{\sum_{t=1}^T \omega_t \cdot V_t \cdot \gamma^t}{\sum_{t=1}^T V_t \cdot \gamma^t} \quad (9)$$

Furthermore, the avoidance of externalities due to the discharge of untreated wastewater to the environment can also be included in the LCOW value, which may help to render a WWTP economically viable. The logic behind this idea, falls in the fact that by treating and reusing wastewater, the pollutants presented in the contaminated water streams are prevented to run into fresh water bodies, rivers or groundwater aquifers. Thus, by defining a monetary value to the prevention of pollutants going into ecosystems, the economic environmental benefits can be internalised [16]. The externalities-related LCOW value $LCOW_{Ext}$ (Equation 10) can be obtained as follows:

$$LCOW_{Ext} = \frac{\sum_p^P \sum_{t=1}^T m_p \cdot B_p \cdot V_t \cdot \gamma^t}{\sum_{t=1}^T V_t \cdot \gamma^t} \quad (10)$$

Where m_p represents the concentration of pollutant of class p avoided with the treatment of one cubic meter of wastewater (kg/m^3), and B_p the environmental benefit of avoiding one kilogram of pollutant p running into the environment ($\$/\text{kg}$).

9. Clusters

The 40 population and cropland clusters identified are presentd in Figure 7.

Clusters are numbered from 0 to 39, yielding 40 agglomerations including each population and cropland areas. Every cluster is tagged with a number and colored to make them stand out from others.

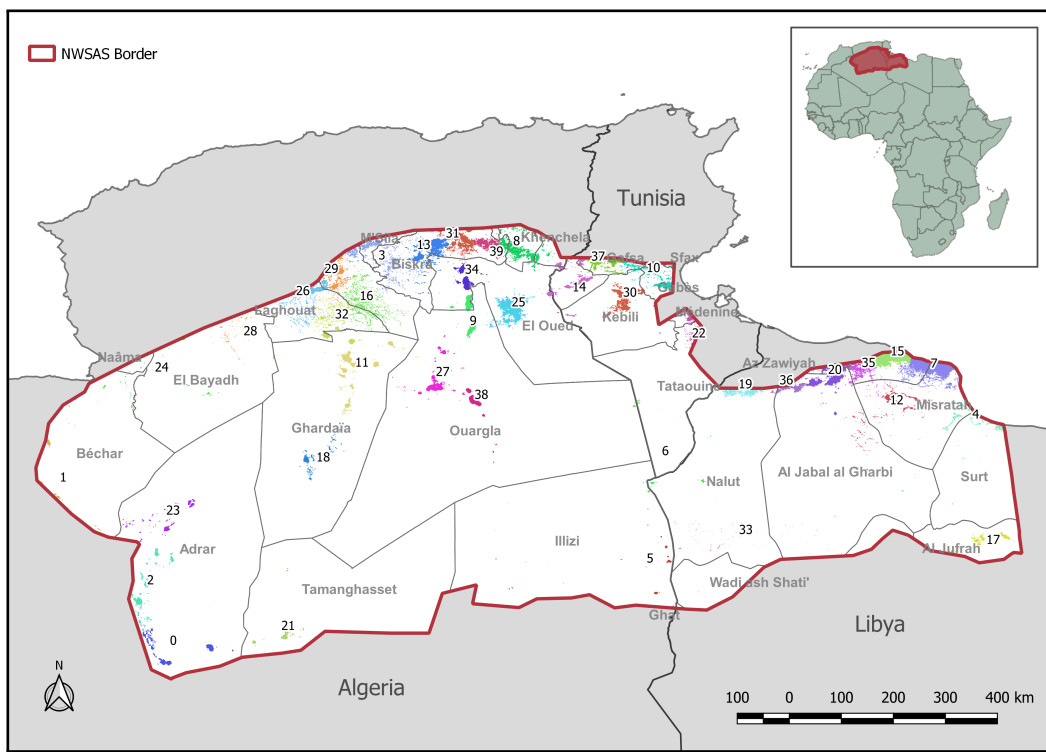


Figure 7. Population and cropland clusters.

10. Water extractions and reuse per cluster

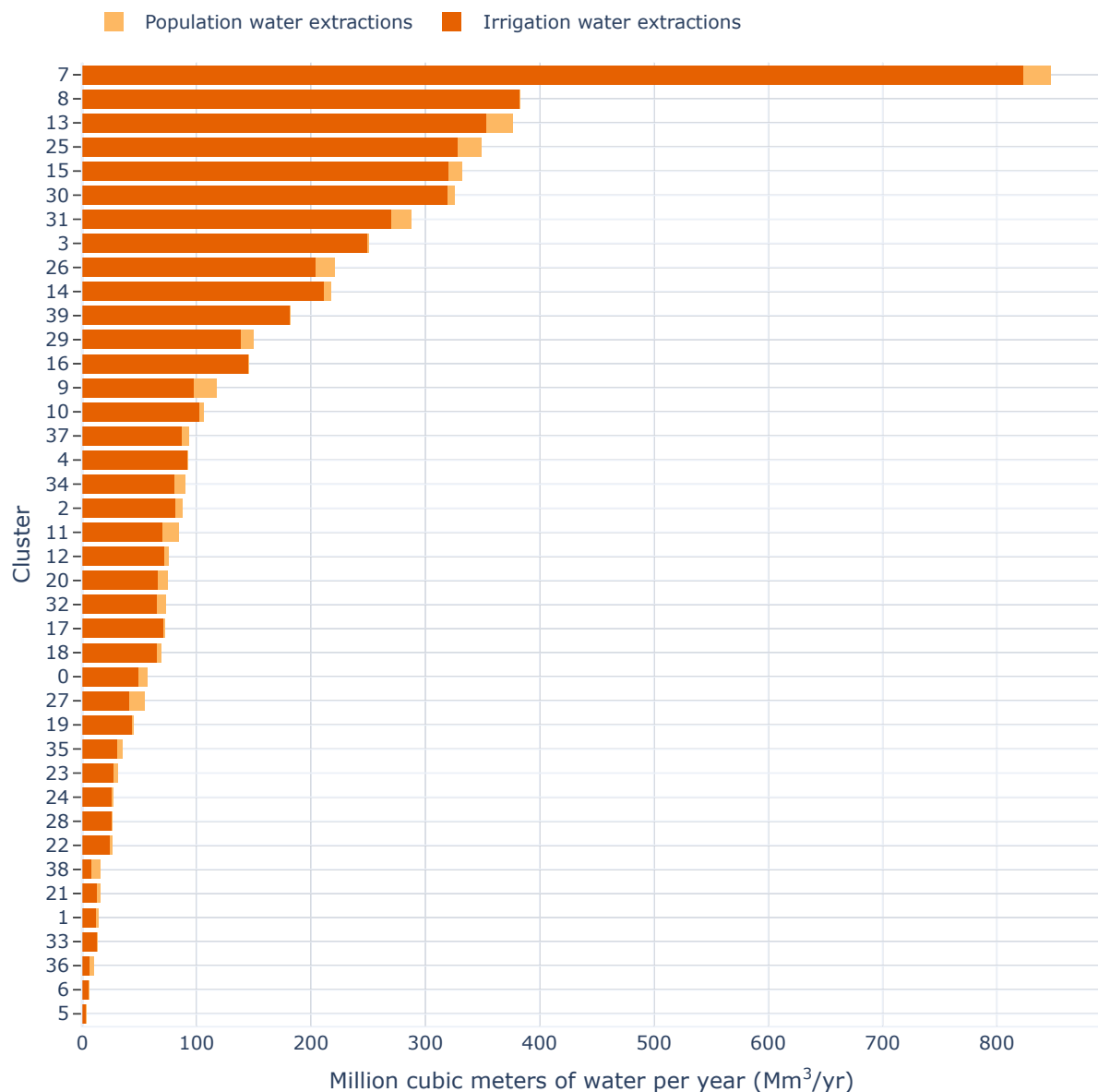
Figure 8 shows the water extractions for agricultural irrigation and population consumption per cluster for the Baseline scenario.

Cluster 7 represents by far, the largest amount of water extractions, this cluster is a combination of population and agricultural irrigation areas from the Al Marqab and Misratah provinces in Libya. It is followed by cluster 8 comprising mainly agricultural irrigation areas of the Khenchela province in Algeria. Then follows cluster 13 and 25 from the northern part of Algerian portion of the basin and cluster 15 of the Al Marqab province in Libya.

All points inside the Biskra province are subdivided into clusters number 13, 31, 39 and 3, which combined represent the major water extractions of the region. However when analysed individually, their impact is reduced, being cluster 13 the most representative.

Overall, Algeria accounts for most of the water extractions, comprising clusters 8, 13, 25, 31, 3 and 26, which rank inside the 10 highest water consumers.

The activity of Tunisia inside the basin is low in comparison with the other two countries. The most representative cluster is number 30 in Kebili, ranking 6 in water extractions

**Figure 8.** Water extractions by cluster. Baseline scenario.

In figure Figure 9 the extractions per sector and treated wastewater reused by source is shown for each cluster for the Subsidized agricultural water and low population water scenario. The clusters, are organized from high to low value of total water extractions.

Again, cluster 7 represents the largest amount of water extractions. It is followed by clusters 15, 8, 25 and 13. It is interesting to notice that the rankings of those clusters in the overall water extractions, changed from the Baseline to the subsidized scenario with water reuse.

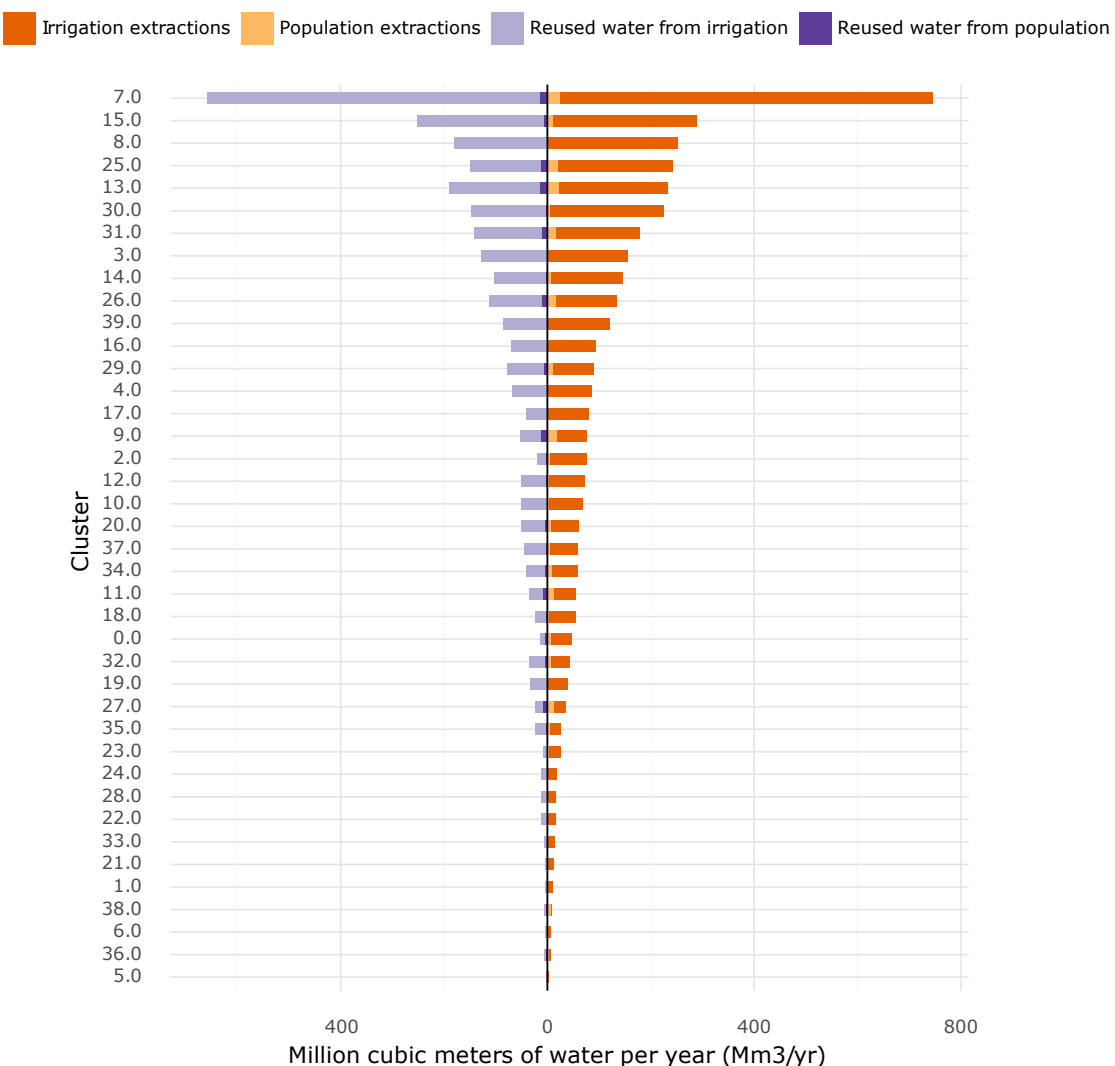


Figure 9. Water extractions and reuse by cluster. Subsidized agricultural water extractions and low population water demand scenario. At left: reused water after reclaim, treatment and allocation classified by population and irrigation source. At right: overall water extractions classified by population and irrigation use.

Figure 10 shows water extractions for the Subsidized agricultural water and high population water scenario. It presents an almost exact behaviour as the previous case, with slightly higher extractions due to the higher population demand and some clusters swapping places in the low ends as clusters 38 and 1.

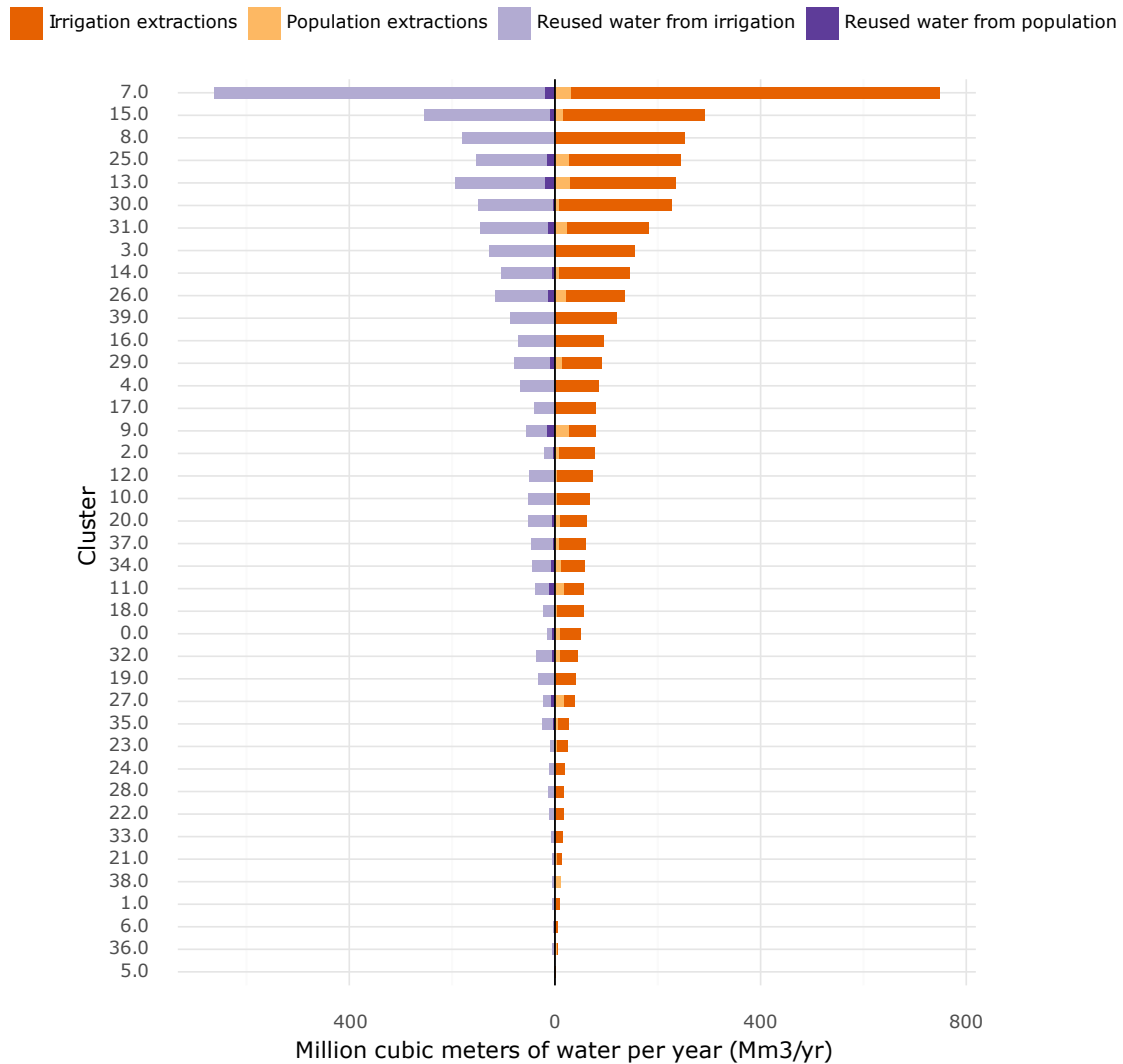


Figure 10. Water extractions and reuse by cluster. Subsidized agricultural water extractions and high population water demand scenario. At left: reused water after reclaim, treatment and allocation classified by population and irrigation source. At right: overall water extractions classified by population and irrigation use.

Figure 11 shows water extractions for the free agricultural water and low population water scenario. It presents an almost exact behaviour as the subsidez case, but with higher extractions due to the lower agricultural water demand. Again some clusters swapped places as clusters 13 and 25.

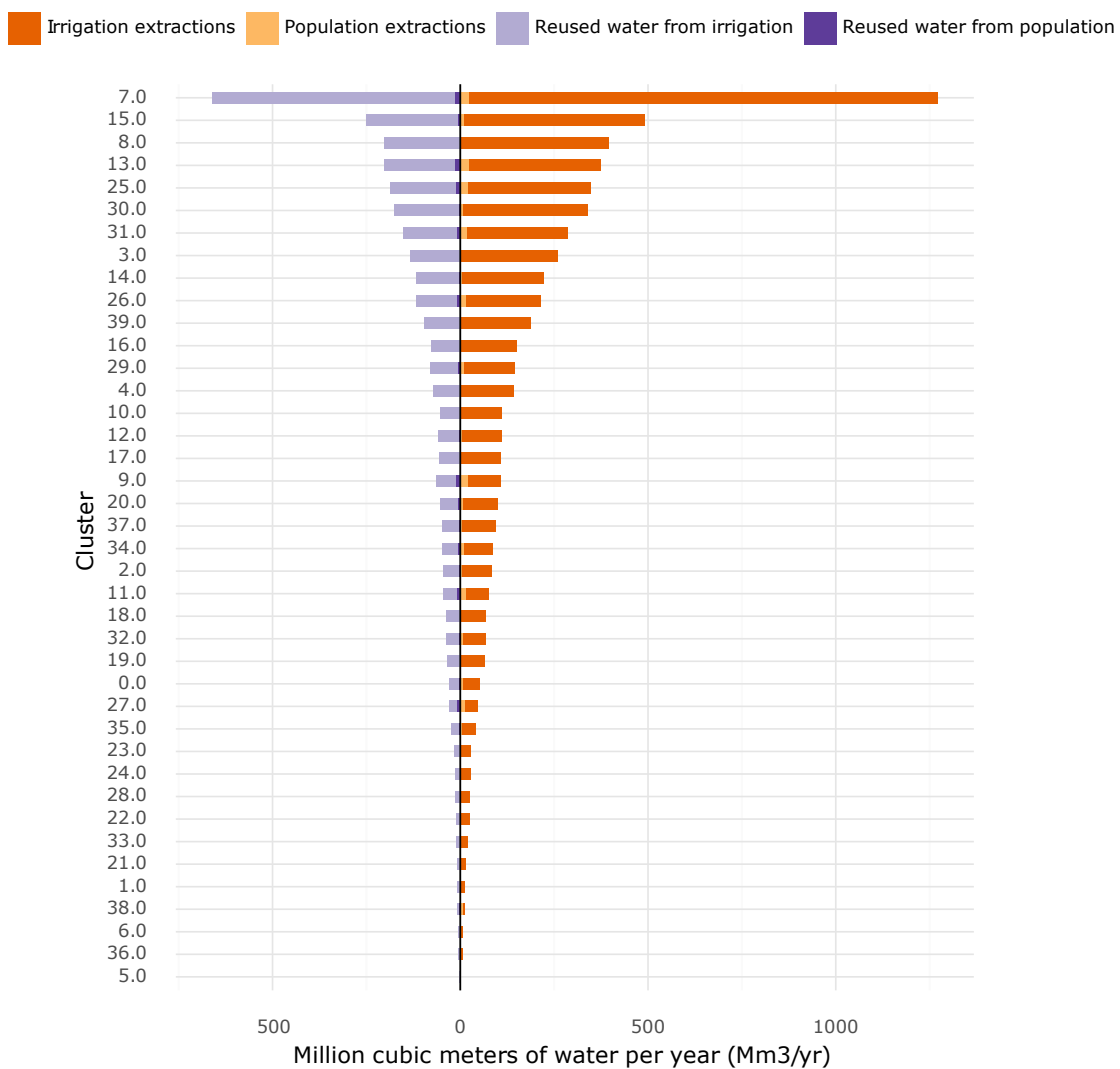


Figure 11. Water extractions and reuse by cluster. Free agricultural water extractions and low population water demand scenario. At left: reused water after reclaim, treatment and allocation classified by population and irrigation source. At right: overall water extractions classified by population and irrigation use.

Figure 12 shows water extractions for the free agricultural water and high population water scenario. It presents an almost exact behaviour as the previous case, but with slightly higher extractions due to the higher population demand.

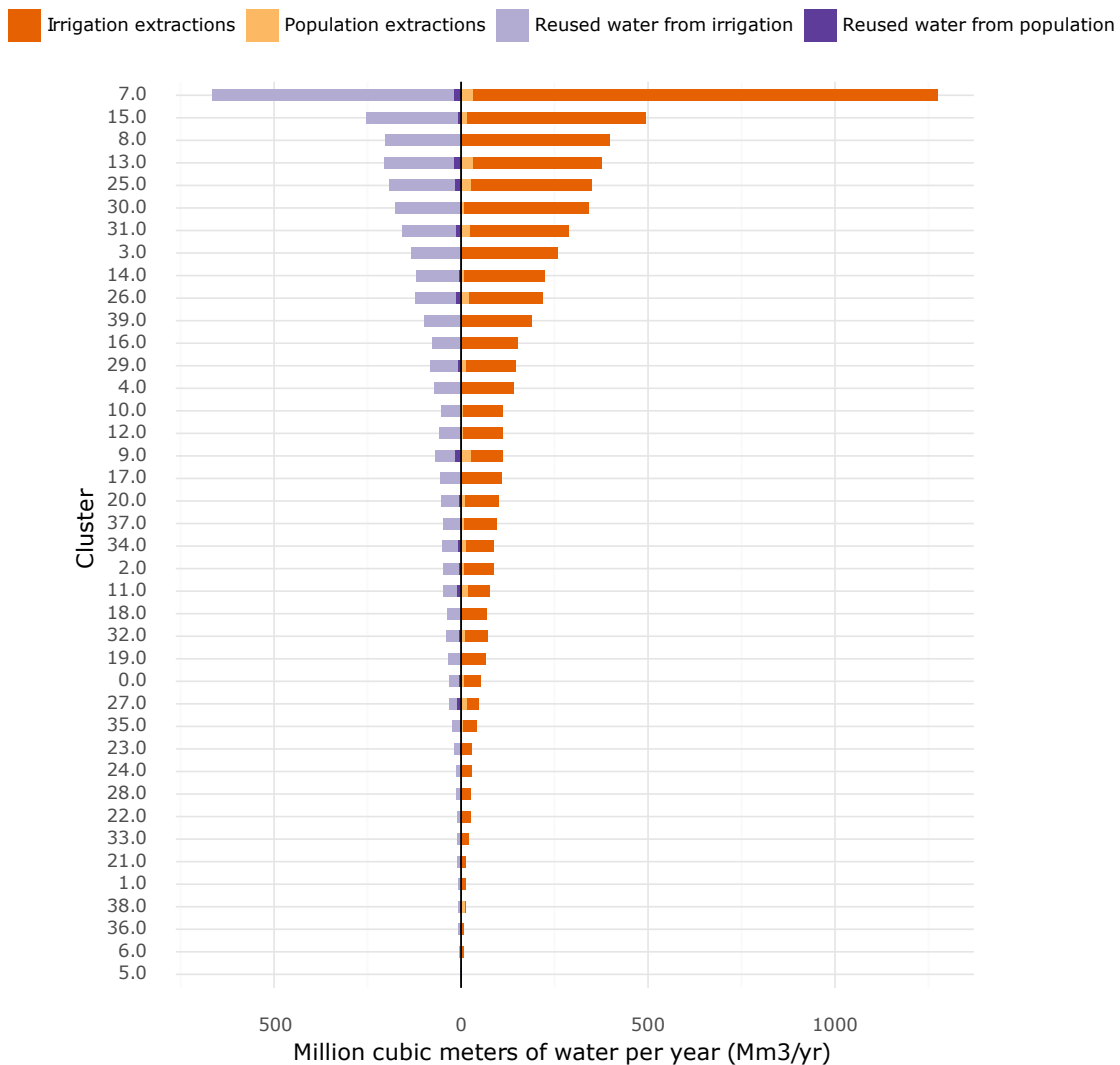


Figure 12. Water extractions and reuse by cluster. Free agricultural water extractions and high population water demand scenario. At left: reused water after reclaim, treatment and allocation classified by population and irrigation source. At right: overall water extractions classified by population and irrigation use.

Finally, water extraction for the private agricultural regime and low to high population water demand, are presented in figures 13 and 14 respectively. Water extractions are much lower in this scenario compared to the free agricultural water scenarios, however the differences are not that high with the subsidized ones. This is due to the higher amount of available water for reuse in the subsidized scenarios, which can be seen in the left part of the graphs. Furthermore, the clusters rankings were the same as for the subsidized cases.

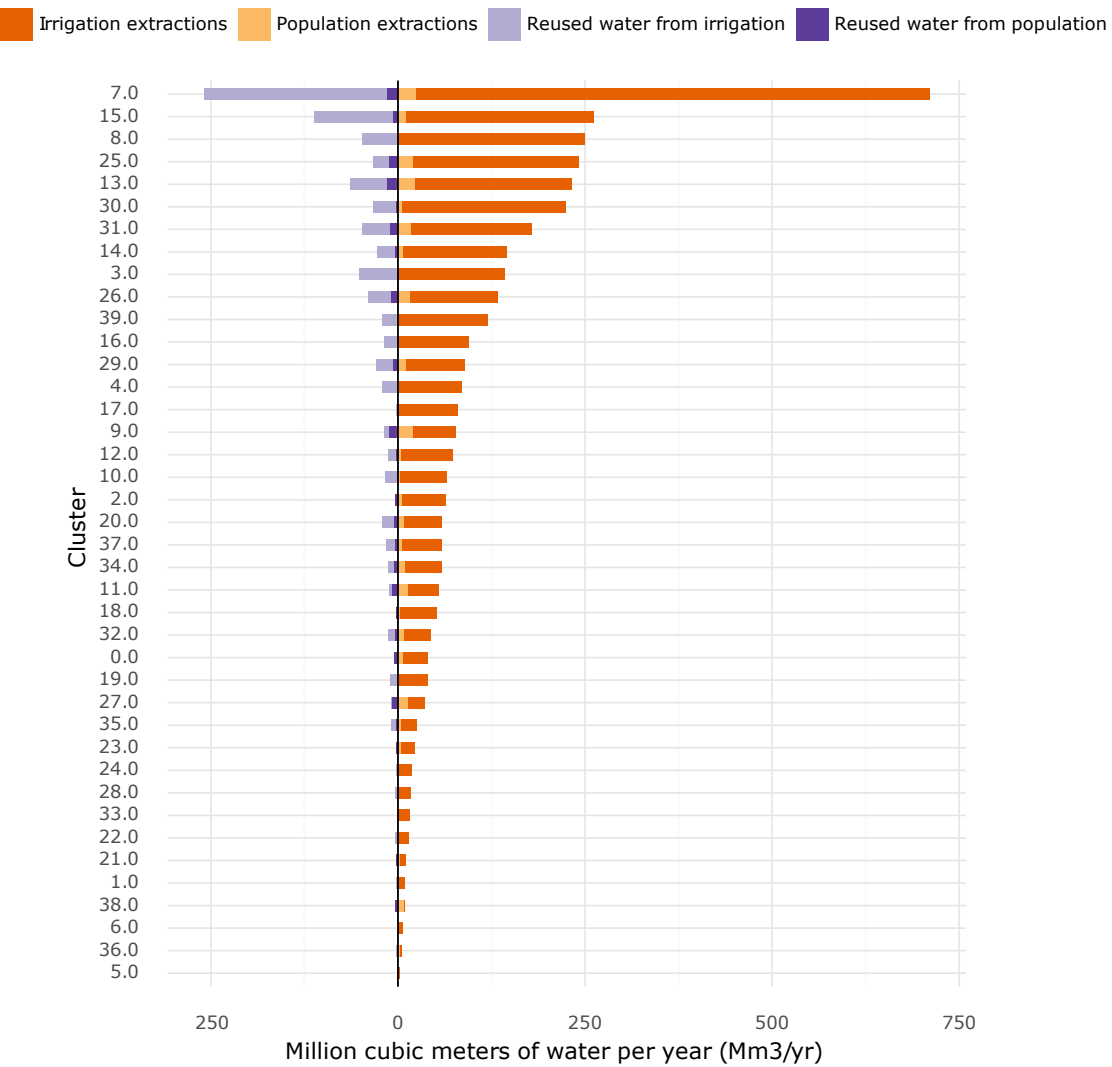


Figure 13. Water extractions and reuse by cluster. Private agricultural water extractions and low population water demand scenario. At left: reused water after reclaim, treatment and allocation classified by population and irrigation source. At right: overall water extractions classified by population and irrigation use.

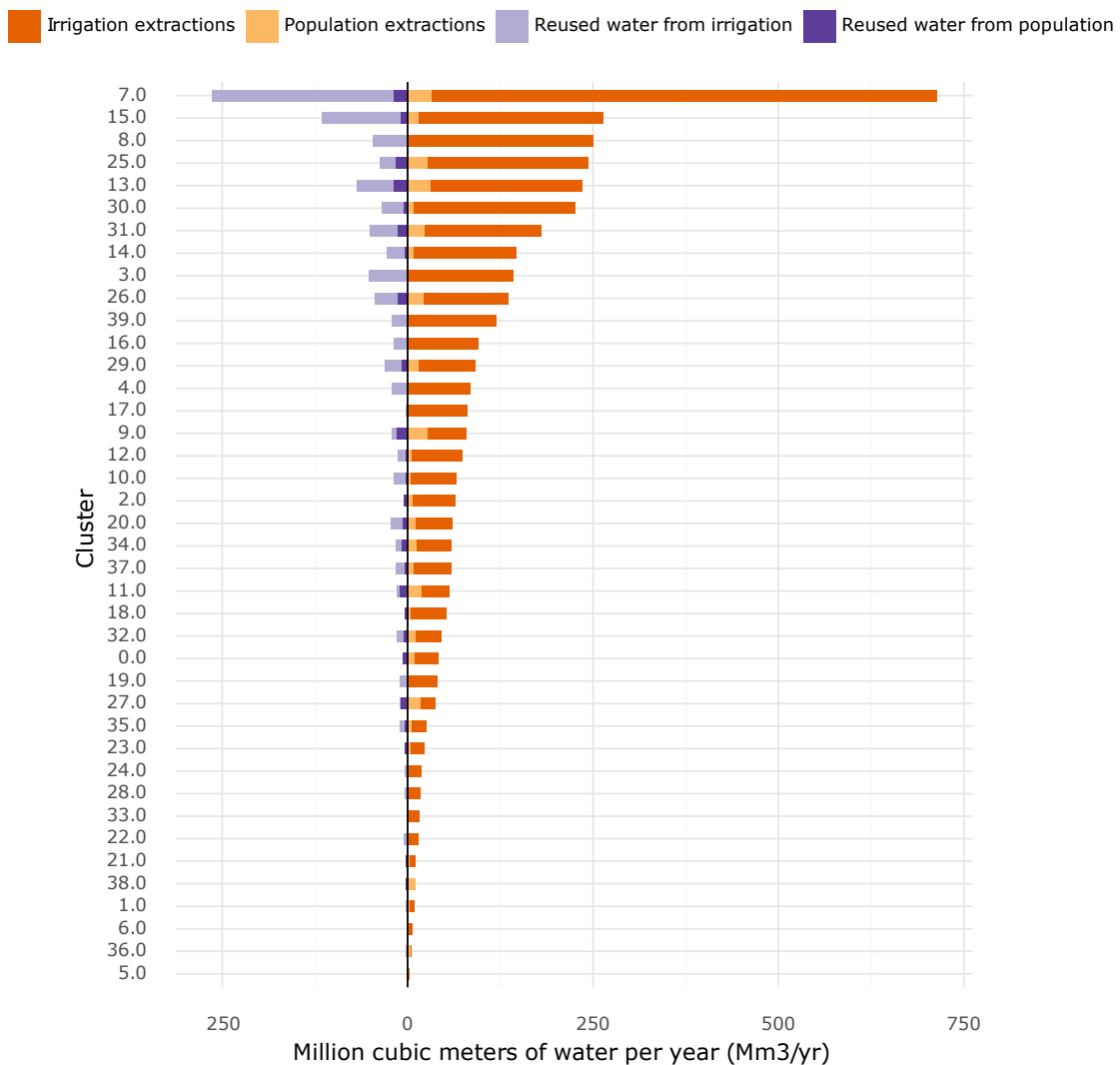


Figure 14. Water extractions and reuse by cluster. Private agricultural water extractions and high population water demand scenario. At left: reused water after reclaim, treatment and allocation classified by population and irrigation source. At right: overall water extractions classified by population and irrigation use.

11. Energy demand per cluster

In this section, additional results concerning the energy requirements for water pumping, water desalination and wastewater treatment are presented.

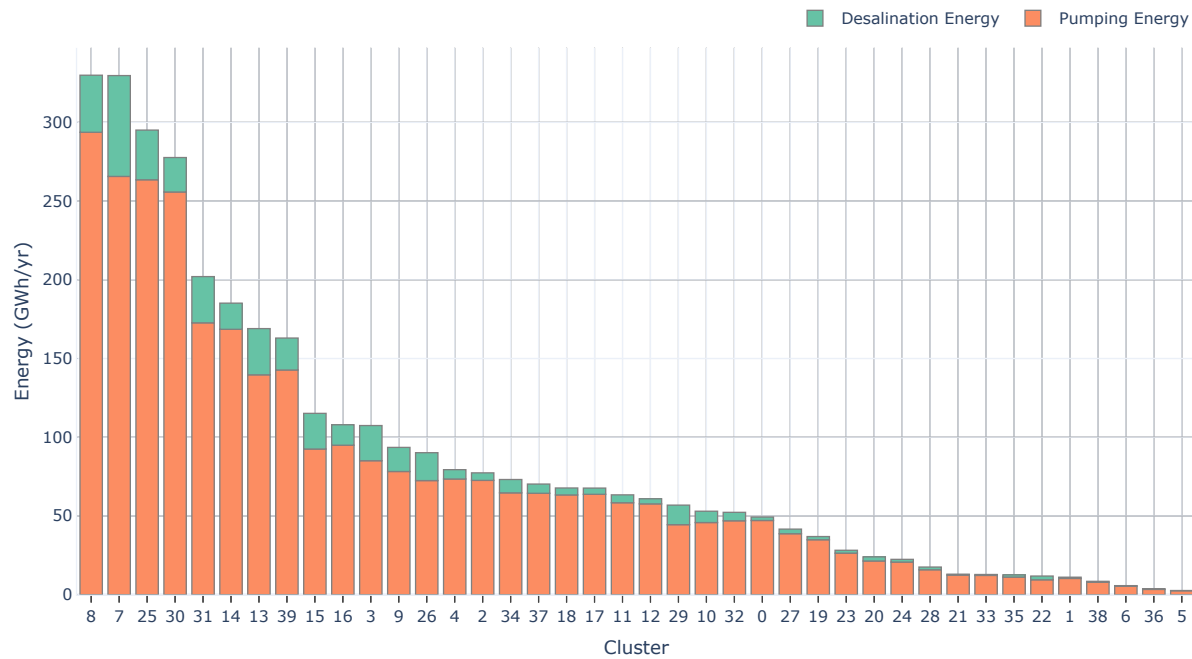


Figure 15. Annual energy demand by cluster in the Baseline scenario.

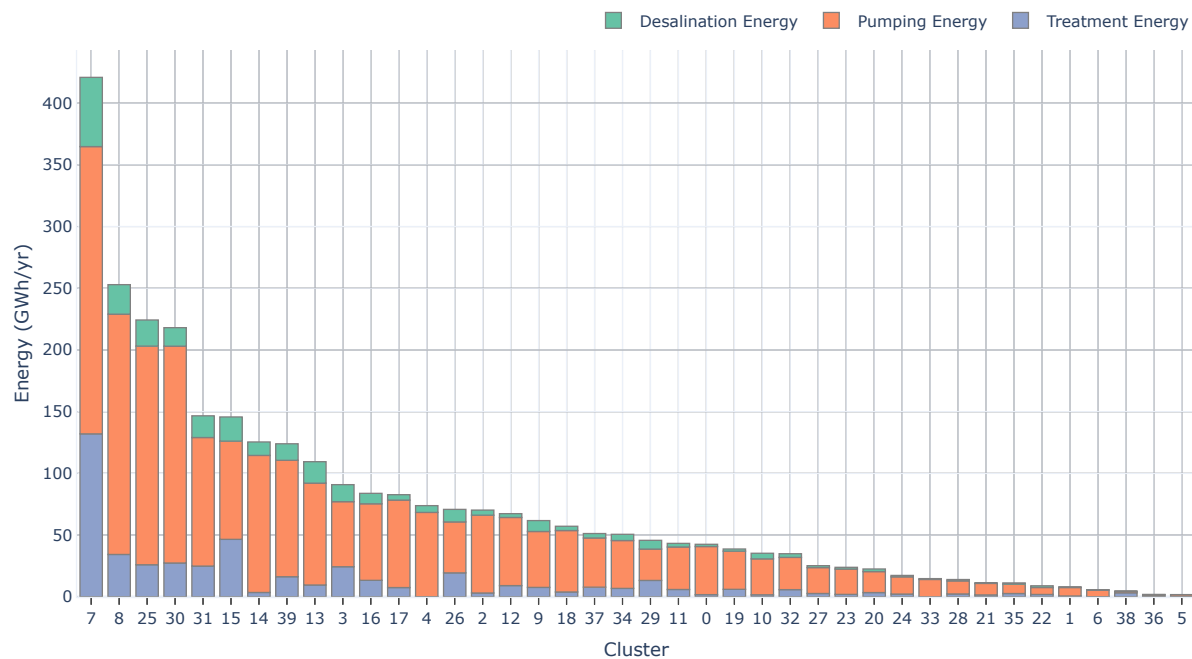


Figure 16. Annual energy demand by cluster in the subsidized agricultural water and low population water scenario.

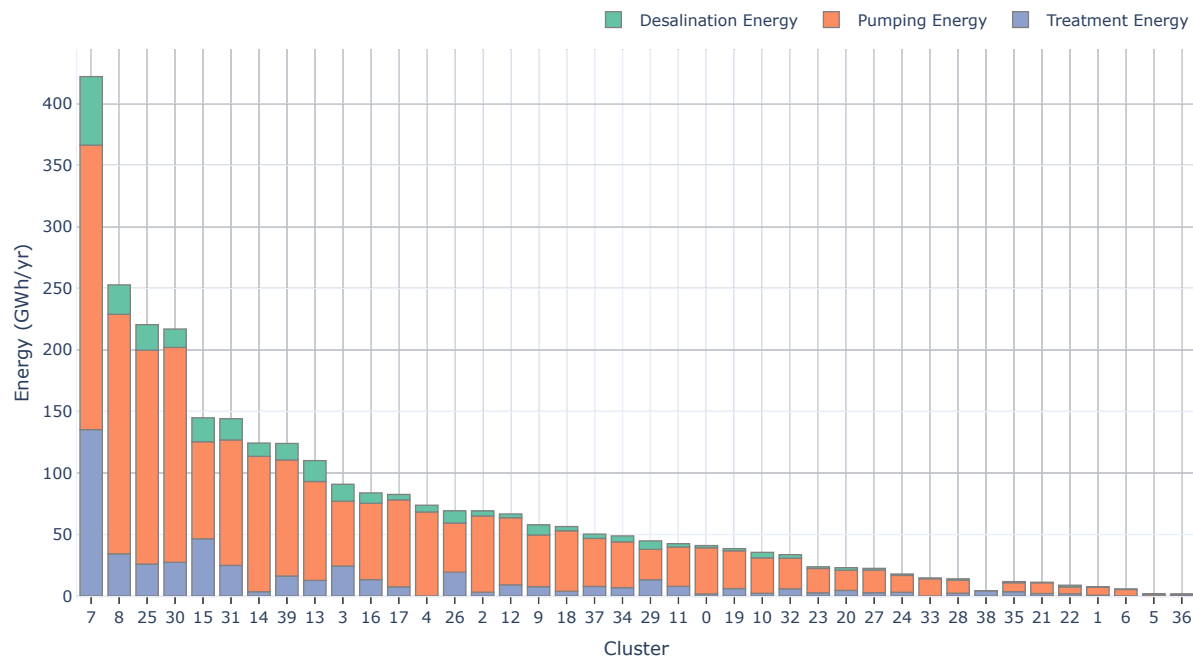


Figure 17. Annual energy demand by cluster in the subsidized agricultural water and high population water scenario.

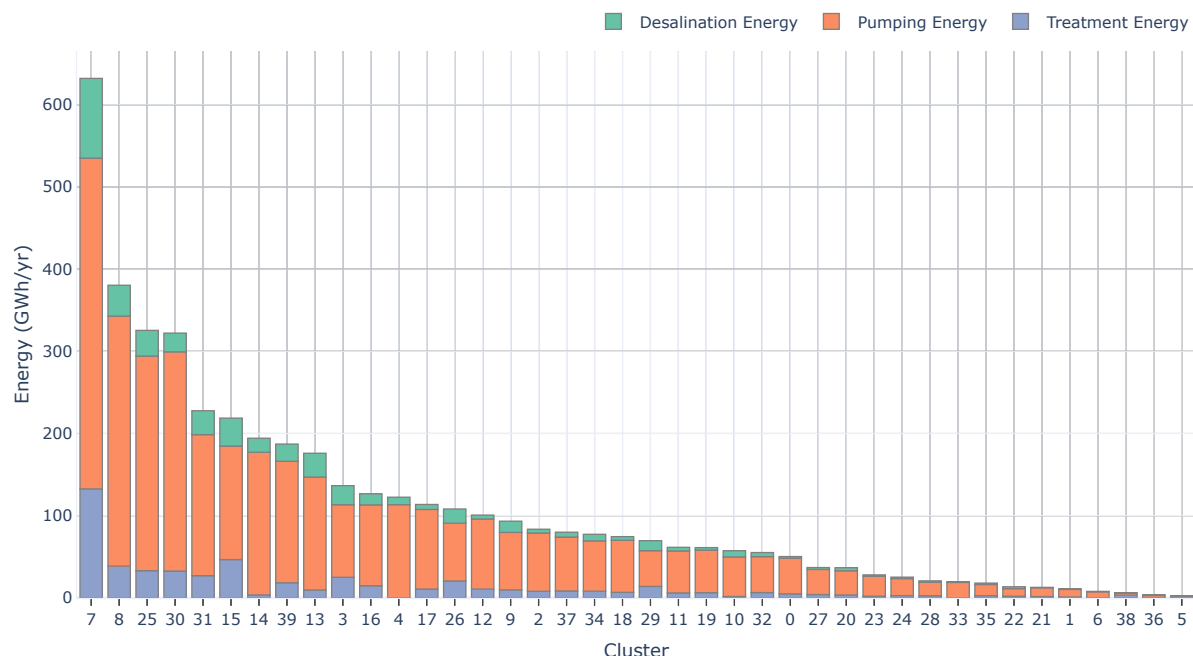


Figure 18. Annual energy demand by cluster in the free agricultural water and low population water scenario.

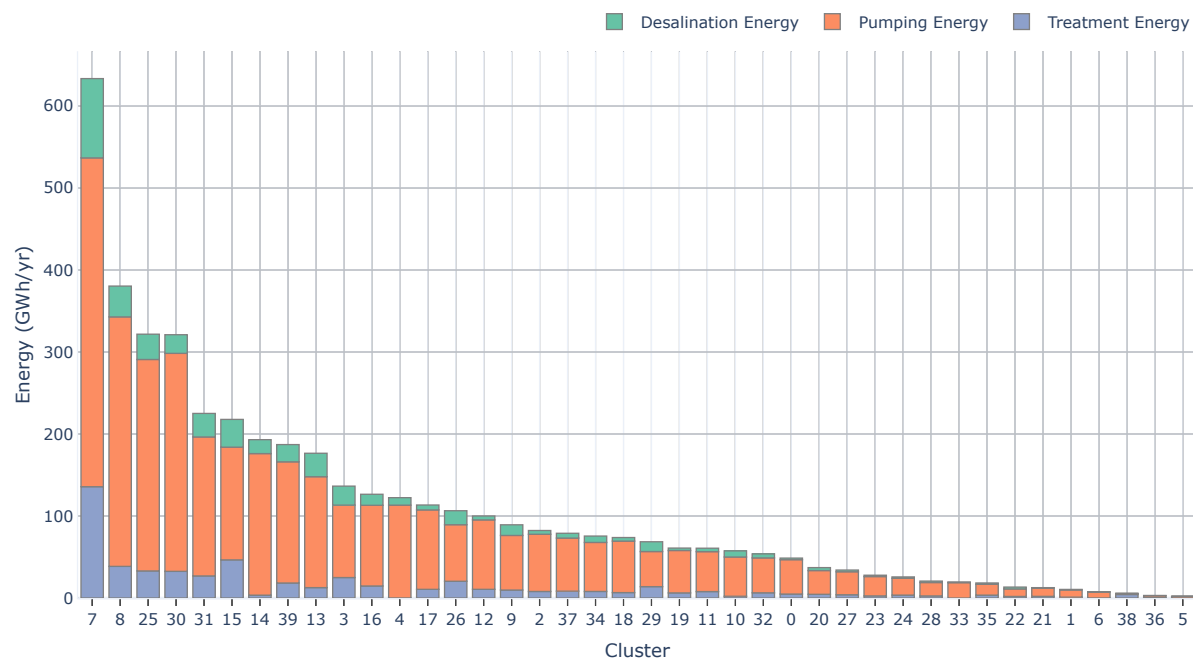


Figure 19. Annual energy demand by cluster in the free agricultural water and high population water scenario.

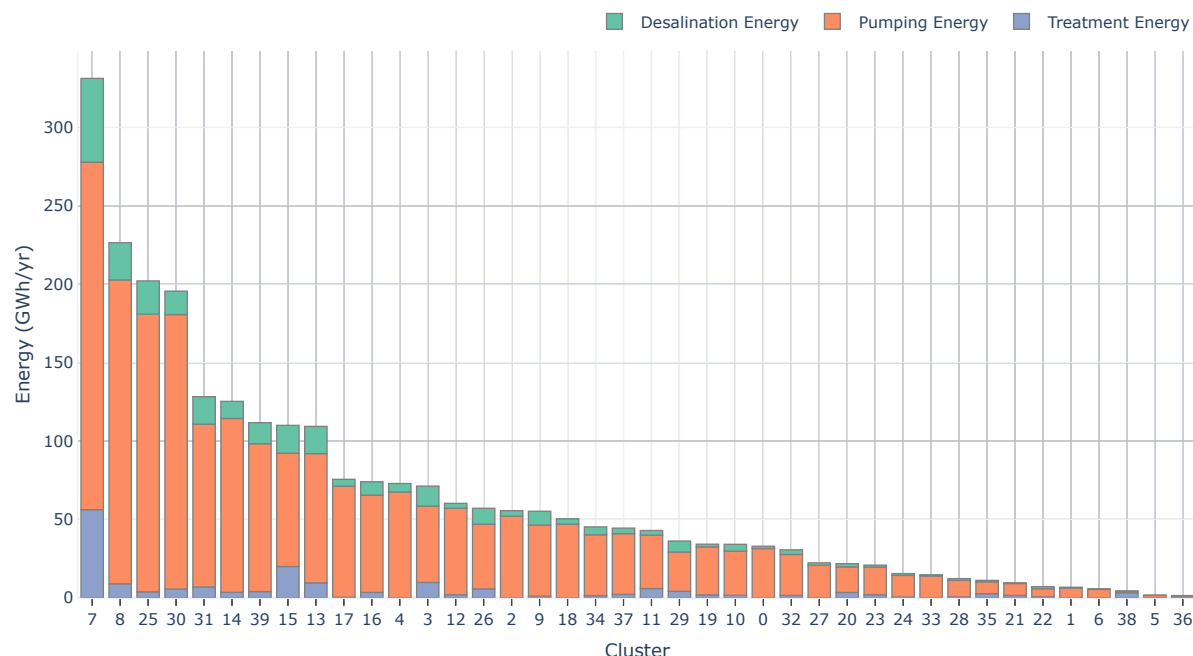


Figure 20. Annual energy demand by cluster in the private agricultural water and low population water scenario.

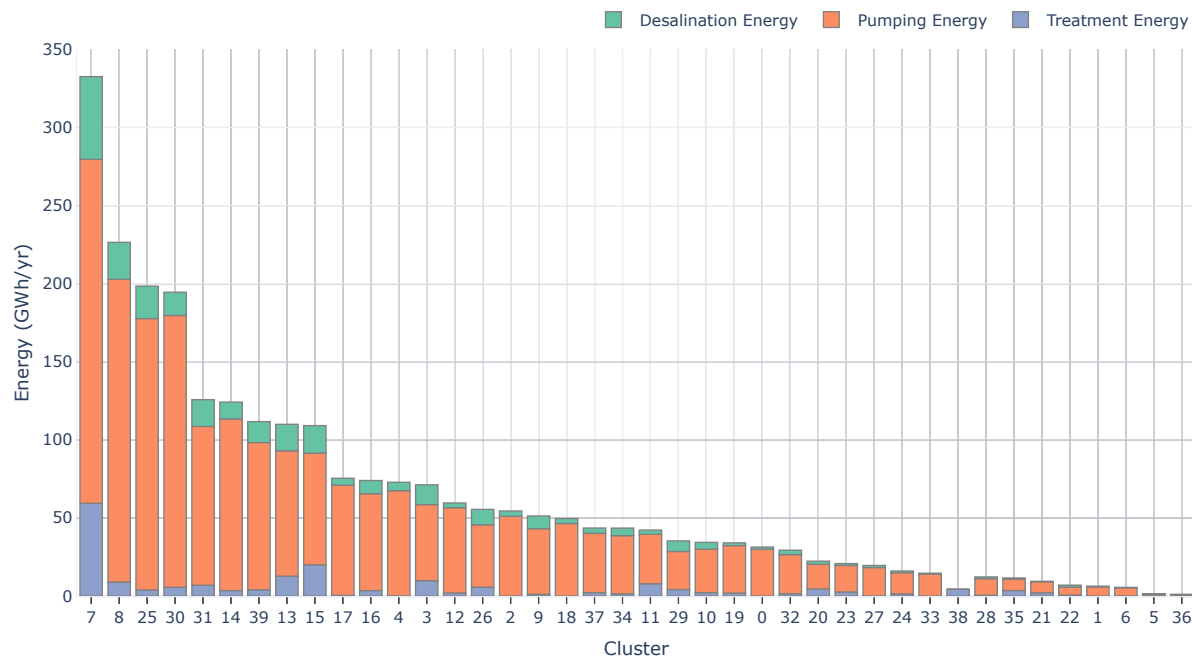


Figure 21. Annual energy demand by cluster in the private agricultural water and high population water scenario.

References

- [1] Catherine Linard, Marius Gilbert, Robert W. Snow, Abdisalan M. Noor, and Andrew J. Tatem. Population Distribution, Settlement Patterns and Accessibility across Africa in 2010. *PLOS ONE*, 7(2):1–8, 2012. doi: 10.1371/journal.pone.0031743.
- [2] A M MacDonald, H C Bonsor, B É Ó Dochartaigh, and R G Taylor. Quantitative maps of groundwater resources in Africa. *Environmental Research Letters*, 7(2): 024009, 2012. ISSN 1748-9326. doi: 10.1088/1748-9326/7/2/024009.
- [3] Humanitarian Information Unit, United States Government. AfricaAmericas LSIB Polygons Simplified. Technical report, United States Government, 2017.
- [4] GADM. Algeria, Tunisia and Libya country boundaries spatial data. <https://gadm.org/index.html>, 2018. Accessed: 2018-08-15.
- [5] IGRAC (International Groundwater Resources Assessment Centre). Transboundary Aquifers of the World [map]. Edition 2015. Scale 1 : 50 000 000. <https://gadm.org/index.html>, 2015. Accessed: 2018-08-15.
- [6] Jonathan de Ferranti. African Digital Elevation Data. <http://viewfinderpanoramas.org/dem3.html>, 2014. Accessed: 2018-08-15.
- [7] ESA Climate Change Initiative - Land Cover project. S2 prototype LC 20m map of Africa 2016. <http://2016africanlandcover20m.esrin.esa.int/>, 2017. Accessed: 2018-08-15.

- [8] WorldClim - Global Climate Data. <http://www.worldclim.org/>, 2020.
- [9] M. Chaouki, A. Zeddouri, and S. Hadj-Said. Study of the Behavior of Some Pollutants and the Vulnerability to Chemical Contamination of Groundwater in the Region of Ouargla (Southeast Algeria). *Energy Procedia*, 36:1043–1049, 2013. ISSN 1876-6102. doi: 10.1016/j.egypro.2013.07.119. URL <http://www.sciencedirect.com/science/article/pii/S1876610213012058>. TerraGreen 13 International Conference 2013 - Advancements in Renewable Energy and Clean Environment.
- [10] GeoData Institute, University of Southampton. Africa population count data, 2015. URL www.worldpop.org.
- [11] OSS. *For a Better Valorization of Irrigation Water in the SASS Basin: Diagnosis and Recommendations*. Sahara and Sahel Observatory, 2015. ISBN 978-9973-856-87-6. NWSAS.
- [12] Meriem Naimi-Ait-Aoudia and Ewa Berezowska-Azzag. Household water consumption in Algiers facing population growth. Water and Cities, Managing a Vital Relationship. *Proceedings of the 50th ISOCARP Congress, Urban Transformations, Cities and Water*, page 12, 9 2014.
- [13] Sahara and Sahel Observatory (OSS). Socio-economic aspects of irrigation in the SASS basin. A better water valorization for sustainable management of the basin. Technical report, Sahara and Sahel Observatory, 2014.
- [14] Golam Saleh Ahmed Salem, So Kazama, Shamsuddin Shahid, and Nepal C. Dey. Groundwater-dependent irrigation costs and benefits for adaptation to global change. *Mitigation and Adaptation Strategies for Global Change*, 2017. ISSN 1573-1596. doi: 10.1007/s11027-017-9767-7. External.
- [15] Robert S Ayers and Dennis W Westcot. *Water quality for agriculture*, volume 29. Food and Agriculture Organization of the United Nations Rome, 1985.
- [16] M. Molinos-Senante, M. Garrido-Baserba, R. Reif, F. Hernández-Sancho, and M. Poch. Assessment of wastewater treatment plant design for small communities: Environmental and economic aspects. *Science of The Total Environment*, 427-428: 11–18, 2012. ISSN 00489697. doi: 10.1016/j.scitotenv.2012.04.023.
- [17] Pratima Singh, Cynthia Carliell-Marquet, and Arun Kansal. Energy pattern analysis of a wastewater treatment plant. *Applied Water Science*, 2(3):221–226, 2012. ISSN 2190-5495. doi: 10.1007/s13201-012-0040-7.
- [18] Renan Barroso Soares. Comparative Analysis of the Energy Consumption of Different Wastewater Treatment Plants. *International Journal of Architecture, Arts and Applications*, 3(6):79, 2017. ISSN 2472-1107. doi: 10.11648/j.ijaaa.20170306.11.
- [19] F. Hernández-Sancho, M. Molinos-Senante, and R. Sala-Garrido. Cost modelling for wastewater treatment processes. *Desalination*, 268(1):1–5, 2011. ISSN 0011-9164. doi: 10.1016/j.desal.2010.09.042.

- [20] A.K. Plappally and J.H. Lienhard V. Energy requirements for water production, treatment, end use, reclamation, and disposal. *Renewable and Sustainable Energy Reviews*, 16(7):4818–4848, 2012. ISSN 1364-0321. doi: 10.1016/j.rser.2012.05.022.
- [21] James A. Roumasset and Christopher Wada. Energy Costs and the Optimal Use of Groundwater. Allied Social Science Association (ASSA) Annual Meeting, January 3-5, 2014, Philadelphia, PA 161892, Agricultural and Applied Economics Association, 2013.
- [22] Ashlynn S. Stillwell and Michael E. Webber. Predicting the Specific Energy Consumption of Reverse Osmosis Desalination. *Water*, 8(12):601, December 2016. ISSN 2073-4441. doi: 10.3390/w8120601. WOS:000392480200054.
- [23] S. Aminfarid, F.T. Davidson, and M.E. Webber. Multi-layered spatial methodology for assessing the technical and economic viability of using renewable energy to power brackish groundwater desalination. *Desalination*, 450:12–20, January 2019. ISSN 00119164. doi: 10.1016/j.desal.2018.10.014.
- [24] John C. Crittenden, R. Rhodes Trussell, David W. Hand, Kerry J. Howe, and George Tchobanoglous. *MWH's Water Treatment: Principles and Design*. John Wiley & Sons, Inc., 2012. ISBN 978-1-118-13147-3 978-0-470-40539-0. doi: 10.1002/9781118131473.
- [25] A.J. Karabelas, C.P. Koutsou, M. Kostoglou, and D.C. Sioutopoulos. Analysis of specific energy consumption in reverse osmosis desalination processes. *Desalination*, 431:15 – 21, 2018. ISSN 0011-9164. doi: 10.1016/j.desal.2017.04.006. "Desalination, energy and the environment" in honor of Professor Raphael Semiat.
- [26] Stefan Reichelstein and Michael Yorston. The prospects for cost competitive solar PV power. *Special section: Long Run Transitions to Sustainable Economic Structures in the European Union and Beyond*, 55:117–127, 2013. ISSN 0301-4215. doi: 10.1016/j.enpol.2012.11.003.